ISSN 1674-1056
http://cpb.iphy.ac.cn
http://iopscience.iop.org/cpb
中国物理 B
Chinese Physics
中国物理 Chinese Physics B

A new four-dimensional chaotic system with first Lyapunov exponent ≈ 22, hyperbolic curve and circular paraboloid types of equilibria and its switching synchronization by an adaptive global integral sliding mode control

Jay Prakash Singh, Binoy Krishna Roy, Zhouchao Wei(魏周超)
Citation: Chin. Phys. B . 2018, 27(4): 040503. **doi:** 10.1088/1674-1056/27/4/040503

Journal homepage: http://cpb.iphy.ac.cn; http://iopscience.iop.org/cpb

What follows is a list of articles you may be interested in

Effects of intrinsic and extrinsic noises on transposons kinetics

Alssadig A M Yousif, Lulu Lu(鹿露露), Mengyan Ge(葛梦炎), Ying Xu(徐莹), Ya Jia(贾亚)
Chin. Phys. B . 2018, 27(3): 030501. **doi:** 10.1088/1674-1056/27/3/030501

Generalized Chaplygin equations for nonholonomic systems on time scales

Shi-Xin Jin(金世欣), Yi Zhang(张毅)
Chin. Phys. B . 2018, 27(2): 020502. **doi:** 10.1088/1674-1056/27/2/020502

Topological horseshoe analysis and field-programmable gate array implementation of a fractional-order four-wing chaotic attractor

En-Zeng Dong(董恩增), Zhen Wang(王震), Xiao Yu(于晓), Zeng-Qiang Chen(陈增强), Zeng-Hui Wang(王增会)
Chin. Phys. B . 2018, 27(1): 010503. **doi:** 10.1088/1674-1056/27/1/010503

Linear synchronization and circuit implementation of chaotic system with complete amplitude control

Chun-Biao Li(李春彪), Wesley Joo-Chen Thio, Julien Clinton Sprott, Ruo-Xun Zhang(张若洵), Tian-Ai Lu(陆天爱)
Chin. Phys. B . 2017, 26(12): 120501. **doi:** 10.1088/1674-1056/26/12/120501

Multi-scroll hidden attractors and multi-wing hidden attractors in a 5-dimensional memristive system

Xiaoyu Hu(胡晓宇), Chongxin Liu(刘崇新), Ling Liu(刘凌), Yapeng Yao(姚亚鹏), Guangchao Zheng(郑广超)
Chin. Phys. B . 2017, 26(11): 110502. **doi:** 10.1088/1674-1056/26/11/110502

A new four-dimensional chaotic system with first Lyapunov exponent of about 22, hyperbolic curve and circular paraboloid types of equilibria and its switching synchronization by an adaptive global integral sliding mode control*

Jay Prakash Singh[1,†], Binoy Krishna Roy[1], and Zhouchao Wei(魏周超)[2]

[1] *Department of Electrical Engineering, National Institute of Technology Silchar, Silchar* 788010, *India*

[2] *School of Mathematics and Physics, China University of Geosciences, Wuhan* 430074, *China*

(Received 24 October 2017; revised manuscript received 29 December 2017; published online 10 March 2018)

This paper presents a new four-dimensional (4D) autonomous chaotic system which has first Lyapunov exponent of about 22 and is comparatively larger than many existing three-dimensional (3D) and 4D chaotic systems. The proposed system exhibits hyperbolic curve and circular paraboloid types of equilibria. The system has all zero eigenvalues for a particular case of an equilibrium point. The system has various dynamical behaviors like hyperchaotic, chaotic, periodic, and quasi-periodic. The system also exhibits coexistence of attractors. Dynamical behavior of the new system is validated using circuit implementation. Further an interesting switching synchronization phenomenon is proposed for the new chaotic system. An adaptive global integral sliding mode control is designed for the switching synchronization of the proposed system. In the switching synchronization, the synchronization is shown for the switching chaotic, stable, periodic, and hybrid synchronization behaviors. Performance of the controller designed in the paper is compared with an existing controller.

Keywords: new hyperchaotic system, maximum chaos, an infinite number of equilibria, hidden attractors, switching synchronization, global sliding mode control

PACS: 05.45.–a, 05.45.Gg, 05.45.Jn **DOI:** 10.1088/1674-1056/27/4/040503

1. Introduction

Lyapunov exponents play an important role in the characteristic of a dynamical system. Many chaotic or hyperchaotic systems have been reported in various fields.[1–8] The disorderness of a chaotic system is defined by its first Lyapunov exponent.[9,10] Applicability of a chaotic/hyperchaotic system is also governed by the magnitude of the highest Lyapunov exponent.[9,11,12] Thus, developing a chaotic system with the largest first Lyapunov exponent is more interesting in comparison with systems having small Lyapunov exponents. The nature of equilibria depicts the dynamical behavior of a system.[13–17] Recently many chaotic and hyperchaotic systems having different shapes of equilibrium points are reported.[13–17] The investigation of different shaped equilibrium points in chaotic systems is also an interesting research area.

Depending on the types of attractors, available chaotic and hyperchaotic systems are classified as: (i) chaotic systems with self-excited attractors[10,18] and (ii) chaotic systems with hidden attractors.[19–21] A self-excited attractor has a basin of attraction that is associated with an unstable equilibrium point, whereas a hidden attractor has a basin of attraction that does not intersect with small neighborhoods of any equilibrium points.[19–21] The chaotic attractors in the systems with only stable equilibria[15,22] or with no equilibria[23] are called hidden attractors.[21,24–26] Recently, the chaotic systems with an infinite number of equilibria (line/curve/plane shaped equilibria) are also classified into the category of hidden attractors chaotic systems.[26] The study of chaotic systems with hidden attractors is important because they can lead to unexpected and disastrous behaviors with small changes in dynamics as in aeroplane wings, electromechanical systems, bridge,[16,27] etc. The literature was searched to find the availability of 4D chaotic/hyperchaotic systems with many equilibria, and the outcome is listed in Table 1. It is observed from Table 1 that the 4D hyperchaotic/chaotic system with a hyperbolic curve and circular paraboloid equilibria is not available in the literature. Thus, designing of a hyperchaotic/chaotic system with a hyperbolic curve and circular paraboloid equilibria is considered as a worthy motivation of the present work.

Four-dimensional chaotic/hyperchaotic systems have complex dynamical structure and perform better in real life applications compared with the 3D chaotic systems because 4D systems have more disorderness and complexity. In the last decade, various hyperchaotic systems are reported with multiple positive Lyapunov exponents.[34,35] It is also seen in the literature that different methods are reported for developing a hyperchaotic system with multiple positive Lyapunov exponents like (i) by using state feedback control,[36] (ii) the ad-

*One of the authors (Dr. Zhouchao Wei) was supported by the National Natural Science Foundation of China (Grant No. 11772306).

†Corresponding author. E-mail: jayprakash1261@gmail.com

© 2018 Chinese Physical Society and IOP Publishing Ltd

dition of an extra term,[37] (iii) coupling,[38], (iv) parameter perturbation,[39] (v) some more,[34,35] etc. Shen *at al.*[34,35] reported a systematic methodology for constructing a hyperchaotic system with the desired number of positive LEs. However, developing a four-dimensional chaotic system that has the largest first Lyapunov exponent compared with all the existing 3D and 4D chaotic systems is a worthy motivation for this research work.

Table 1. Categorization of the reported 4D chaotic and hyperchaotic systems with an infinite number of equilibrium points.

4D system	Shape of equilibria of system	Reference
4D chaotic system	plane of equilibria	[28]
4D hyperchaotic system	line of equilibria	[29], [30]
4D hyperchaotic system	curve of equilibria	[31]
4D memristive hyperchaotic system	line of equilibria	[33], [37]
4D chaotic/hyperchaotic system	hyperbolic curve and circular paraboloid equilibria	this work

In this paper, a new 4D chaotic system which also has hyperchaotic behavior is reported. Following are the contributions and novelty of the paper in comparison with the existing literature on this topic:

(i) A new 4D chaotic system is developed which has the highest first Lyapunov exponent in comparison with many reported 3D and 4D chaotic systems in the literature.

(ii) The new system has a hyperbolic curve and a circular paraboloid type of equilibria. Such a system is not available in the literature.

(iii) The new system has all zero eigenvalues at a particular equilibrium point.

(iv) The new system exhibits multistability.

(v) Switching synchronization phenomenon is proposed for the synchronization of the new system.

(vi) An adaptive global integral sliding mode control (SMC) is designed for the switching synchronization of the proposed system.

The rest of this paper is organized as follows. Section 2 describes the dynamics of the new chaotic system. Numerical analyses of the new system are shown in Section 3. Circuit implementation of the new system is discussed in Section 4. In Section 5 we discuss the switching synchronization phenomena for the proposed system. Results and discussions for the switching synchronization are presented in Section 6. Finally, the conclusions of this paper are summarized in Section 7.

2. A new chaotic system with the highest first Lyapunov exponent

This section describes the generation of the new chaotic system having the largest positive LE. Various analyses using theoretical and numerical tools for the new system are also given in this section.

2.1. Dynamics of the new system

Li *et al.*[40] reported a 3D chaotic system with a line of equilibria whose dynamics is described in the following equation

$$\begin{cases} \dot{x} = ay - yz - xz, \\ \dot{y} = bxz, \\ \dot{z} = y^2 - cz^2. \end{cases} \tag{1}$$

The system in Eq. (1) has chaotic behavior with $a = 1$, $b = 4$, and $c = 0.3$. It has two equilibrium points at $E1\,(0,\ \pm\sqrt{c}, 1)$ and $E2\,(x^*,\ 0,\ 0)$. Thus, system (1) has a line of equilibria for $E2\,(x^*,\ 0,\ 0)$. A new hyperchaotic system is generated by using a state feedback control in the third state of system (1). The dynamics of the new system is given in the following

$$\begin{cases} \dot{x} = ay - yz - xz, \\ \dot{y} = bxz, \\ \dot{z} = y^2 - cz^2 + w^2 - p, \\ \dot{w} = -dx. \end{cases} \tag{2}$$

The system (2) has the largest positive first Lyapunov exponent with parameters $a = 40$, $b = 105$, $c = 0.152$, $d = 0.2$, and $p = 0.1$. Lyapunov exponents of the new system for the above sets of parameters are $L_i = (22.1301, 0, -0.0028, -25.6512)$ and the Kaplan–Yorke dimension is $D_{KY} = 3.862$. The positive LE of 22.1301 is the largest among all the reported 3D and 4D chaotic systems in the literature.

The divergence of system (2) is given as follows:

$$\nabla v = \frac{\partial \dot{x}}{\partial x} + \frac{\partial \dot{y}}{\partial y} + \frac{\partial \dot{z}}{\partial z} + \frac{\partial \dot{w}}{\partial w} = -(1 + 2c)z. \tag{3}$$

Thus, the hyper-volume of system (2) contracts exponentially with respect to time at a rate of $(1+2c)z$, for $z, c > 0$ and converges to zero as time tends to infinity.

System (2) is invariant under the coordinate transformation $(x, y, z, w) \to (-x, -y, z, -w)$. Therefore, system (2) has symmetry about the z axis. Thus, the system may have a symmetric pair of coexisting attractors.

2.2. Equilibrium points

Equilibrium points of system (2) are obtained by equating the derivative of each state to zero. After some calculations, we obtained the equilibrium point as $E((a-z)y = 0, 0, z,\ y^2 - cz^2 + w^2 - p = 0)$. Thus, the equilibrium points are

$$\begin{cases} E_{1,2} = \left(0,\ 0,\ z^*,\ \pm\sqrt{c(z^*)^2 + p}\right), \\ E_{3,4} = \left(0,\ y^*,\ a,\ \pm\sqrt{ca^2 - (y^*)^2 + p}\right). \end{cases} \tag{4}$$

The shape of equilibria using $E_{1,2}$ and $E_{3,4}$ is shown in Figs. 1(a) and 1(b), respectively. The equilibria $E_{1,2}$ have a shape similar to $w^2/p^2 - z^2/q^2 = 1$ (hyperbolic curve). Equilibria $E_{3,4}$ has a shape similar to $y^2/p^2 + w^2/q^2 = 1$ (circular paraboloid).[41]

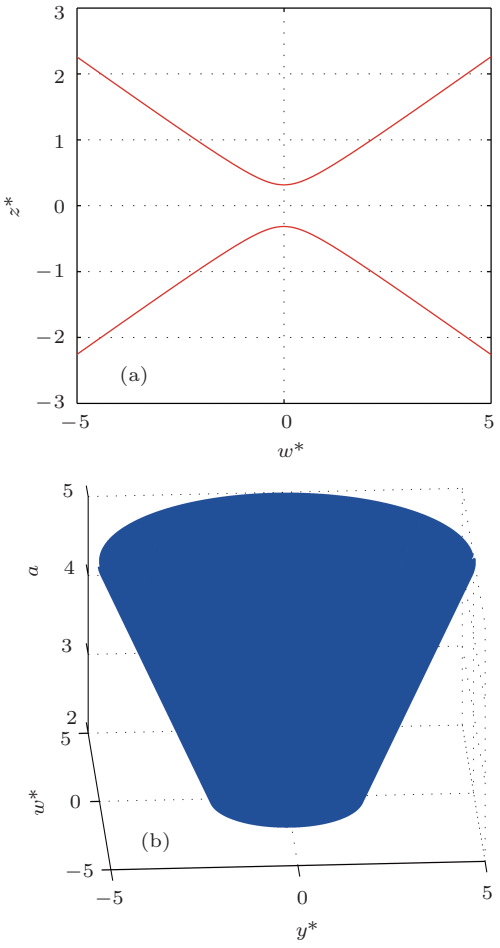


Fig. 1. (color online) Shape of equilibrium points of system (2).

The Jacobian matrix of system (2) is defined as

$$J = \begin{bmatrix} -z^* & (a-z^*) & -(x^*+y^*) & 0 \\ bz^* & 0 & bx^* & 0 \\ 0 & 2y^* & -2cz^* & 2w^* \\ -d & 0 & 0 & 0 \end{bmatrix}. \tag{5}$$

The characteristics polynomials corresponding to the equilibria $E_{1,2}$ and $E_{3,4}$ using the Jacobian J are written as

$$\begin{aligned} P_1 &= \lambda^4 + \lambda^3\left(z^*(1+2c)\right) + \lambda^2\left(b(z^*)^2 + 2c(z^*)^2 - abz^*\right) \\ &\quad + \lambda\left(2bc(z^*)^3 - 2abc(z^*)^2\right), \\ P_2 &= \lambda^4 + \lambda^3(a+2ac) + \lambda^2\left(2ca^2\right) \\ &\quad + \lambda\left(2ab(y^*)^2 - dy^*\sqrt{\left(4a^2c - 4(y^*)^2 + 0.4\right)}\right). \end{aligned} \tag{6}$$

The calculation of the eigenvalues corresponding to the equilibria $E_{1,2}$ of the new system is shown below. From Eq. (6), we can obtain

$$\begin{aligned} P_1 = \lambda\Big[&\lambda^3 + \lambda^2\left(z^*(1+2c)\right) + \lambda\left(b(z^*)^2 + 2c(z^*)^2 - abz^*\right) \\ &+ \left(2bc(z^*)^3 - 2abc(z^*)^2\right)\Big] \end{aligned} \tag{7}$$

or it can be written as

$$\begin{cases} P_1 = \lambda(h_1\lambda^3 + h_2\lambda^2 + h_3\lambda + h_4), \\ \lambda_1 = 0; h_1\lambda^3 + h_2\lambda^2 + h_3\lambda + h_4 = 0, \end{cases} \tag{8}$$

where

$$\begin{cases} h_1 = 1, h_2 = z^*(1+2c), \\ h_3 = (b(z^*)^2 + 2c(z^*)^2 - abz^*), \\ h_4 = 2bc(z^*)^3 - 2abc(z^*)^2. \end{cases} \tag{9}$$

Now suppose

$$\begin{cases} A = h_2^2 - 3h_1h_3,\ \ B = h_2h_3 - 9h_1h_4,\ \ C = h_3^2 - 3h_2h_4, \\ \Delta = B^2 - 4AC. \end{cases} \tag{10}$$

The calculations of eigenvalues is shown in the following cases.

Case 1

$$\begin{cases} A = B = 0, \\ \lambda_2 = \lambda_3 = \lambda_4 = (-h_2)/(3h_1); \end{cases} \tag{11}$$

Case 2

$$\begin{cases} \Delta = B^2 - 4AC > 0, \\ \lambda_2 = \dfrac{-h_2 - \sqrt[3]{Y_1} + \sqrt[3]{Y_2}}{3h_1}, \\ \lambda_{3,4} = \dfrac{-h_2 - \dfrac{1}{2}\left(\sqrt[3]{Y_1} + \sqrt[3]{Y_2}\right) \pm \dfrac{\sqrt[3]{3}}{2}\left(\sqrt[3]{Y_1} - \sqrt[3]{Y_2}\right)\mathrm{i}}{3h_1}, \\ Y_{1,2} = Ah_2 + 3h_1\dfrac{-B \pm \sqrt[2]{B^2 - 4AC}}{2}; \end{cases} \tag{12}$$

Case 3

$$\begin{cases} \Delta = B^2 - 4AC = 0, \\ \lambda_2 = \dfrac{-h_2}{h_1} + K, \\ \lambda_{3,4} = \dfrac{-K}{2}, \\ K = \dfrac{B}{A}(A \neq 0); \end{cases} \tag{13}$$

Case 4

$$\begin{cases} \Delta = B^2 - 4AC < 0, \\ \lambda_2 = \dfrac{-h_2 - 2\sqrt{A}\cos(\theta/3)}{3h_1}, \\ \lambda_{3,4} = \dfrac{-h_2 + \sqrt{A}\left[\cos(\theta/3) \pm \sin(\theta/3)\right]}{3h_1}, \\ \theta = \arccos\left(\dfrac{2Ah_2 - 3h_1B}{2\sqrt{A^2}}\right). \end{cases} \tag{14}$$

The calculation of eigenvalues for P_2 can be done in a similar manner. It is seen that the nature of the equilibria $E_{1,2}$ depends upon the values of state variables z and y, respectively. A special case of equilibria $E_{1,2}$ when $z^* = 0$, is $E_{1,2} = (0, 0, 0, \pm 0.31)$, where the eigenvalues of the system are $\lambda_{1,2} = (0, 0, 0, 0)$. Thus, system (2) has an interesting feature having all zero eigenvalues at a particular case of equilibria $E_{1,2}$.

3. Numerical analyses

Dynamical behavior of system (2) with the variation of a parameter and keeping other parameters fixed is evaluated using the Lyapunov spectrum plots. The spectrum is generated by finding the Lyapunov exponents with observation time $T = 2 \times 10^4$ fixed initial conditions $(x(0), y(0), z(0), w(0)) = (0.00001, 0.00001, 0.7, 0.01)$ and by using Wolf *et al.* algorithm.[42] The resulted Lyapunov spectrums are shown in Figs. 2–4. The new system has only chaotic behavior with the variation of parameter p. Thus, its effect on variation is not shown in the paper. It is seen from Figs. 2–4 that the system has different dynamical behaviors like chaotic, periodic, quasi-periodic, and hyperchaotic.

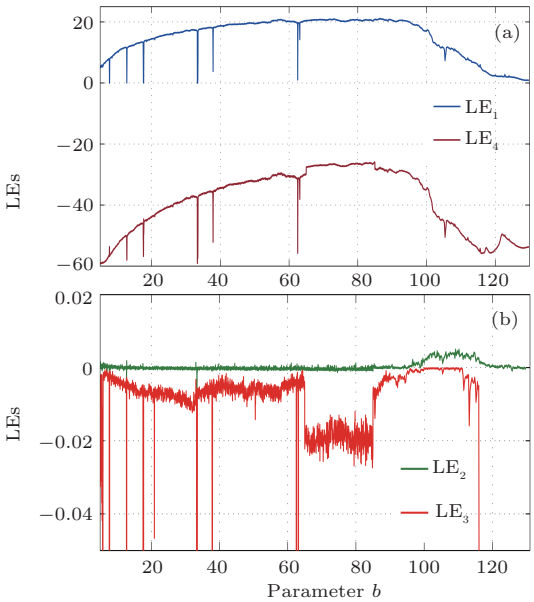


Fig. 2. (color online) Lyapunov spectrum with variation of parameter b of system (2) with $a = 40$, $c = 0.152$, $d = 0.2$, $p = 0.1$ and $b \in [5,\ 135]$.

Here in Figs. 2–4, it is noticed that the system has the largest first Lyapunov exponent. A comparison of the reported highest first Lyapunov exponent systems along with the proposed system is given in Table 2.

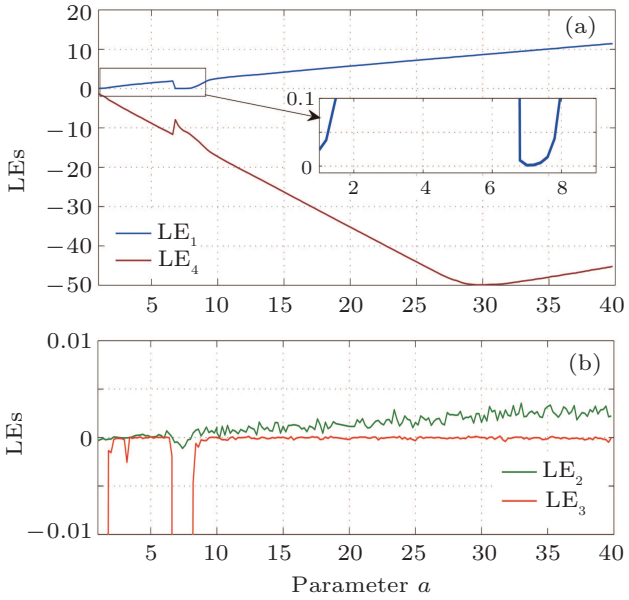


Fig. 3. (color online) The Lyapunov spectrum with variation of the parameter a of the system (2) with parameters $b = 105$, $c = 0.152$, $d = 0.2$, $p = 0.1$, and $a \in [0.1,\ 40]$.

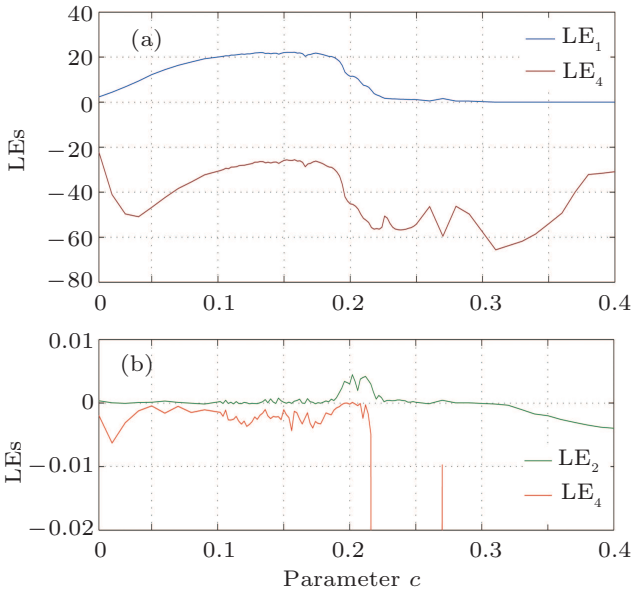


Fig. 4. (color online) The Lyapunov spectrum with variation of the parameter c of the system (2) with parameters $a = 40$, $b = 105$, $d = 0.2$, $p = 0.1$, and $c \in [0.01,\ 0.4]$.

It is seen from Table 2 that system (2) has the largest first positive Lyapunov exponent in comparison with the reported three-dimensional and four-dimensional chaotic systems. It needs to be mentioned that only those chaotic systems are considered for comparison which have the first Lyapunov exponent greater than 10. Further, the highest first Lyapunov exponent of a system is invariant for scaling up or scaling down of the system.

Table 2. Comparison of the first positive Lyapunov exponent based on reported works.

3D/4D	System	Lypunov exponents
3D	[43]	$L_i = (10.45056, 0, -42.36623)$
4D	[12]	$L_i = (11.9258, 0, -4.9358, -58.5255)$
4D	system (2) with $a = 105$, $b = 40$, $c = 0.152$, $d = 0.152$	$L_i = (22.1301, 0, -0.0028, -25.6512)$
4D	system (2) with $a = 100.0$, $b = 40$, $c = 0.152$, $d = 0.2$	$L_i = (17.0902, 0.00143, 0, -34.9012)$

The hyperchaotic attractors of the system (2) with parameters $a = 40$, $b = 105$, $c = 0.152$, and $d = 0.2$ are shown in the following Fig. 5.

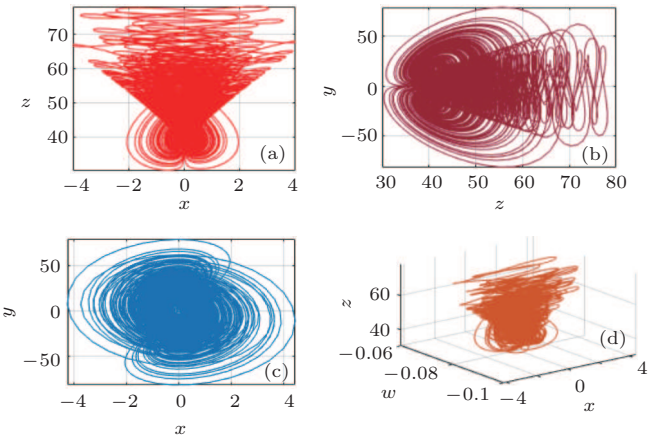


Fig. 5. (color online) Hyperchaotic attractors of system (2) with $a = 40$, $b = 105$, $c = 0.152$, and $d = 0.2$.

The new system shows coexistence of chaotic attractors with the change of initial conditions. The coexistence of chaotic attractors of system (2) are shown in Fig. 6.

Figure 6 is simulated with the following initial conditions

$$(x(0), y(0), z(0), w(0)) = (0.00001, 0.00001, \pm 0.7, 0.01).$$

The Poincaré maps of the system (2) across different sections of planes are shown in Fig. 7. It is evidently seen that the results shown in Figs. 5–7 validate the chaotic behavior of the new system.

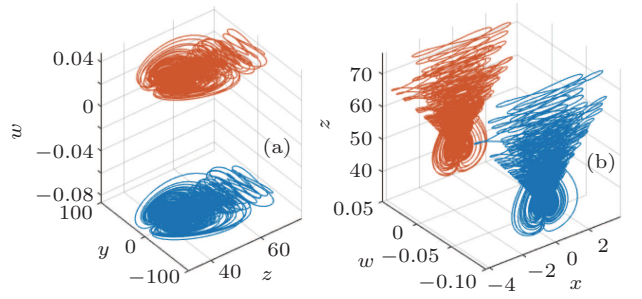


Fig. 6. (color online) Coexistence of chaotic attractors of system (2) with $a = 40$, $b = 105$, $c = 0.152$, $d = 0.2$, $p = 0.1$ and initial conditions $(0.00001, 0.00001, \pm 0.7, 0.01)$ (brown,blue).

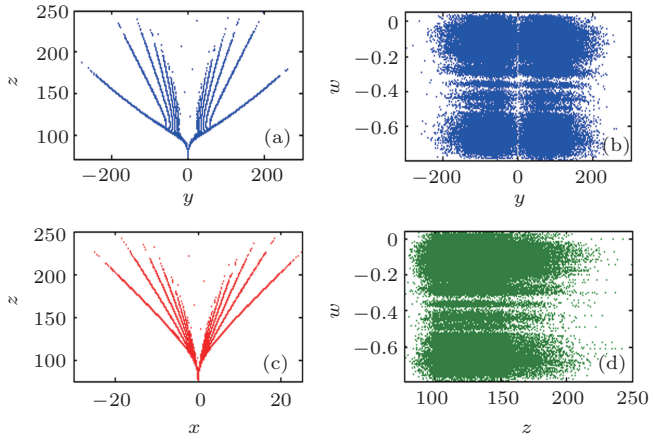


Fig. 7. (color online) Poincaré maps of system (2) with $a = 40$, $b = 105$, $c = 0.2$, $d = 0.2$, $p = 0.1$: across $x = 0$ in panels (a) and (b), and $y = 0$ in panels (c) and (d).

Basins of attraction of the new system across x–y and z–w planes are shown in Fig. 8.

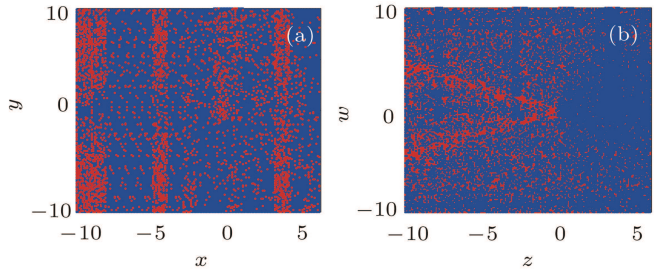


Fig. 8. (color online) The basins of attraction of the new system with $a = 40$, $b = 105$, $c = 0.2$, $d = 0.152$, $p = 0.1$ across (a) x–y plane keeping $z = 0.7$, $w = 0.01$ fixed (b) and z–w planes with $x = 0.0001$, $y = 0.0001$ where red is hyperchaotic and blue is chaotic.

4. Circuit implementation

This section describes the design and construction of an electronic circuit realization of system (2). To validate the mathematical expression of a chaotic system and its applicability in real life, hardware implementation is important and desirable.[26]

Here, the circuit is designed and implemented by using NI multisim software. Four integration lines are considered corresponding to four states of the system. Circuit implementation of system (2) is shown in Fig. 9. The circuit is designed with parameters $a = 5$, $b = 40$, $c = 0.2$, $d = 0.2$, and $p = 0.1$. The circuit equation similar to system (2) can be written as the

following form

$$\begin{cases} \dot{x} = \dfrac{1}{RC_2}\left[\dfrac{R}{R_1}y - \dfrac{R}{R_2}yz - \dfrac{R}{R_3}xz\right], \\ \dot{y} = \dfrac{1}{RC_4}\left[\dfrac{R}{R_4}xz\right], \\ \dot{z} = \dfrac{1}{RC_3}\left[\dfrac{R}{R_7}y^2 - \dfrac{R}{R_9}z^2 + \dfrac{R}{R_8}w^2 - \dfrac{R}{R_{10}}V_1\right], \\ \dot{w} = -\dfrac{1}{RC_1}\left[\dfrac{R}{R_3}x\right], \end{cases} \tag{15}$$

where x, y, z, and w are the outcomes of the integrators U1A, U7A, U5A, U3A, respectively. The circuit equation (15) is similar to system (2) with $\tau = t/RC$, $R = 100$ kΩ, $R_1 = R/a = 20$ kΩ, $R_2 = R/10 = 10$ kΩ, $R_3 = R/10 = 10$ kΩ, $R_4 = R/10b = 0.5$ kΩ, $R_7 = R_8 = R/10 = 10$ kΩ, $R_9 = R/10c = 50$ kΩ, $R_{10} = 1000$ kΩ, $V_1 = 1$ V, $R_{13} = 500$ kΩ, $C_1 = C_2 = C_3 = C_4 = 10$ nF, $a = 5$, $b = 40$, $c = 0.2$, $d = 0.2$, and $p = 0.1$.

Circuit implementation results are shown in Fig. 10. It is observed from this figure that the attractors plot has chaotic behavior and validates with the MATLAB simulation results.

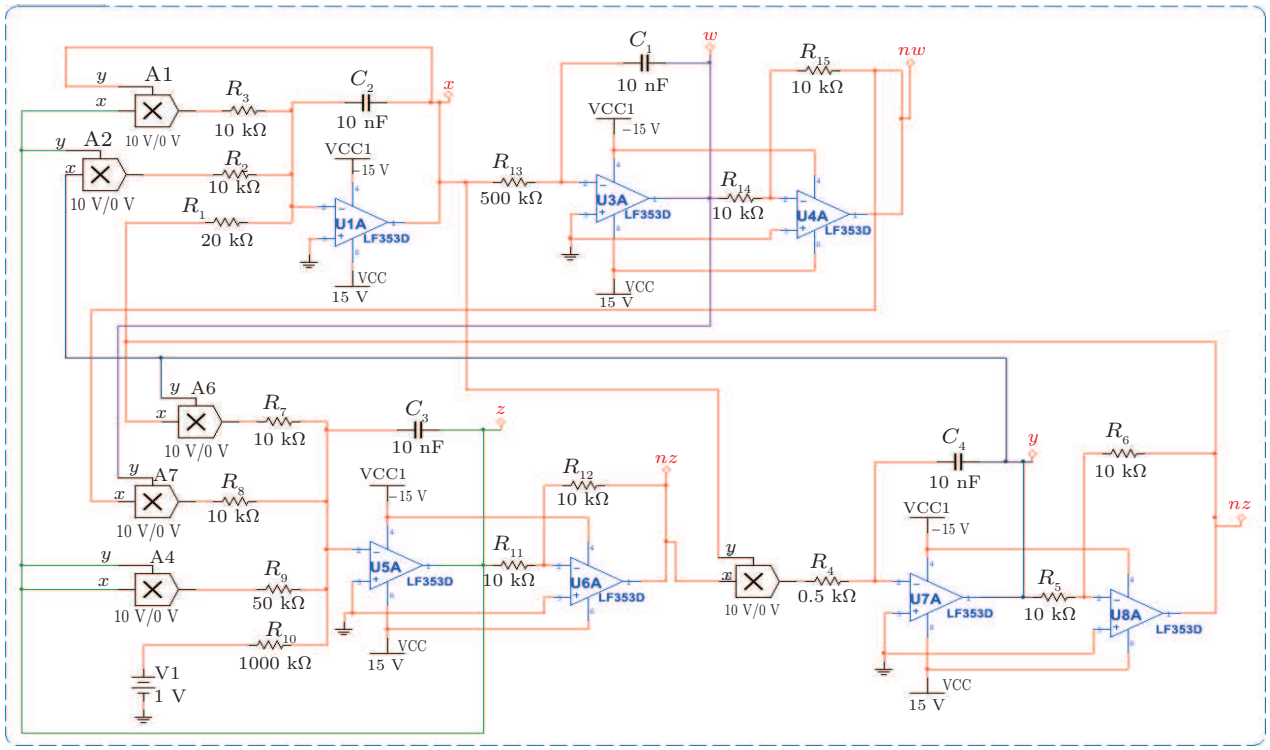


Fig. 9. (color online) Circuit implementation of system (2).

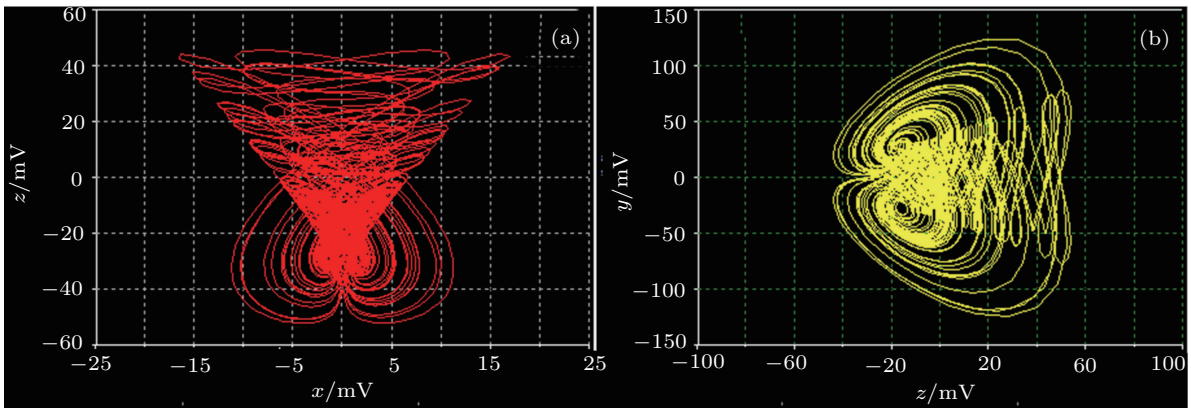


Fig. 10. (color online) Chaotic attractors of system (2): (a) across x–z and (b) across z–y obtained using NI Multisim circuit implementation.

5. Switching synchronization of the new system

Synchronization of a hyperchaotic/chaotic system is one of the most focused applications of hyperchaotic/chaotic systems and studied by various researchers as seen in Refs. [44] and [45]. Various types of synchronization techniques like complete,[46] anti,[46] hybrid,[47] phase,[48] lag,[49] projective synchronization,[50] etc., are reported in the literature. Most of the papers deal with one of the aforesaid synchronization techniques. However, the concept of switching synchronization

may be considered as an interesting research problem. Thus, designing of switching synchronization, which makes the system behavior switch among chaotic states, stable states, periodic states, synchronization and anti-synchronization with a master system, is the motivation of the present research work.

Different control techniques are proposed for the synchronization of a hyperchaotic/chaotic system like active control,[46] sliding mode control (SMC),[51] observer-based control,[52] and hybrid control techniques,[53] etc. Recently, some papers reported with linear and composite control of chaotic systems.[54,55] Among these control techniques, an SMC is considered as a better and effective controller because of its many inherent advantages.[56] Recently, more attention has been paid for overcoming the inherent disadvantages of an SMC like high gain and the chattering problem. An integral SMC is used to solve the high gain problem[56] and reaching time of the sliding surface is reduced by a global SMC.[45] Motivated with the above-stated literature, the aim of this section is to design an adaptive global integral SMC for the multiple switching synchronization of the new system.

The proposed system in Eq. (2) is considered as both master and slave systems. Two control inputs (u_1, u_2) are added in the first and third states of the slave system. The master and slave systems are described in Eqs. (16) and (17), respectively.

$$\begin{cases} \dot{x}_1 = ax_2 - x_2x_3 - x_1x_3 + d_1, \\ \dot{x}_2 = bx_1x_3, \\ \dot{x}_3 = x_2^2 - cx_3^2 + x_4^2 - 0.1 + d_2, \\ \dot{x}_4 = -dx_1, \end{cases} \tag{16}$$

$$\begin{cases} \dot{y}_1 = ay_2 - y_2y_3 - y_1y_3 + d_3 + u_1, \\ \dot{y}_2 = by_1y_3, \\ \dot{y}_3 = y_2^2 - cy_3^2 + y_4^2 - 0.1 + d_4 + u_2, \\ \dot{y}_4 = -dy_1, \end{cases} \tag{17}$$

where d_1, d_2, d_3, and d_4 are the bounded matched disturbances. The synchronization error dynamics between the master and slave systems (16) and (17) is defined as:

$$\begin{cases} \dot{e}_1 = \dot{y}_1 - \dot{x}_1 \\ \quad = ae_2 - y_2y_3 - y_1y_3 + x_2x_3 + x_1x_3 + d_3 - d_1 + u_1, \\ \dot{e}_2 = \dot{y}_2 - \dot{x}_2 = be_1y_3 + bx_1e_3, \\ \dot{e}_3 = \dot{y}_3 - \dot{x}_3 \\ \quad = y_2^2 - cy_3^2 + y_4^2 - x_2^2 + cx_3^2 - x_4^2 + d_4 - d_2 + u_2, \\ \dot{e}_4 = \dot{y}_4 - \dot{x}_4 = -de_1. \end{cases} \tag{18}$$

Asymptotic stability of error dynamics in Eq. (18) is ensured by considering the following integral sliding surfaces as

$$\begin{cases} s_1 = e_1 + \int_0^t (k_1e_1 + be_2y_3 - de_4)\,\mathrm{d}\tau, \\ s_2 = e_3 + \int_0^t (k_2e_3 + bx_1e_2)\,\mathrm{d}\tau, \end{cases} \tag{19}$$

where k_1 and k_2 are positive constants to be decided by the designer of the controller. When the system operates in the sliding surface, it satisfies $\dot{s}_i = 0$. Therefore, using this condition along with Eqs. (18) and (19), the equivalent sliding mode dynamics is written as[56]

$$\begin{cases} \dot{e}_1 = -k_1e_1 - be_2y_3 + de_4, \\ \dot{e}_2 = be_1y_3 + bx_1e_3, \\ \dot{e}_3 = -k_3e_3 + bx_1e_2, \\ e_4 = -de_1. \end{cases} \tag{20}$$

The stability of Eq. (20) is shown by considering a Lyapunov function candidate as

$$V_1(x) = (1/2)(e_1^2 + e_2^2 + e_3^2 + e_4^2).$$

The time derivative of $V_1(x)$ using Eq. (20) is written as

$$\dot{V}_1(x) = -k_1e_1^2 - k_2e_3^2. \tag{21}$$

It is apparent that equation (21) is a negative-definite function. Thus, according to the Lyapunov stability theory, the sliding motion on the sliding surface is asymptotically stable and ensures the convergence of error dynamics to the origin.

In order to achieve the smoother, and chattering free control input and sliding surface, global sliding surfaces are designed as[45]

$$\begin{cases} \sigma_1 = G_1(s_1 - s_1(0)\,\mathrm{e}^{-a_1t}), \\ \sigma_2 = G_2(s_2 - s_2(0)\,\mathrm{e}^{-a_2t}), \end{cases} \tag{22}$$

where $G_1, G_2 > 0$, and $a_1, a_2 > 0$ are the gain constants. $s_1(0)$, and $s_2(0)$ are the initial states of the sliding surfaces s_1 and s_2, respectively.

Now, in order to bring the system trajectory onto the sliding surfaces $\sigma_1 = \sigma_2 = 0$, sliding mode control laws are proposed as:

$$\begin{cases} u_1 = -k_1e_1 - be_2y_3 + de_4 - ae_2 + y_2e_3 + x_3e_2 \\ \qquad + y_1e_3 + x_3e_1 - a_1s_1(0)\,\mathrm{e}^{-a_1t} \\ \qquad - M_1\,\mathrm{sgn}(\sigma_1)\,|\sigma_1|^{\eta_1} - \gamma_1\sigma_1 - \rho_1\tanh(\sigma_1), \\ u_2 = -k_2e_3 - bx_1e_2 - y_2^2 + cy_3^2 - y_4^2 + x_2^2 - cx_3^2 + x_4^2 \\ \qquad - a_2s_2(0)\,\mathrm{e}^{-a_2t} - M_2\,\mathrm{sgn}(\sigma_2)\,|\sigma_2|^{\eta_2} - \gamma_2\sigma_2 \\ \qquad - \rho_2\tanh(\sigma_2), \end{cases} \tag{23}$$

where M_1, M_2, γ_1, γ_2, ρ_1, and ρ_2 are positive gains constants.

Theorem 1 If the slave system in Eq. (17) is controlled by the sliding mode control given in Eq. (23) then its trajectories follow the master system (16) and ensure the asymptotic convergence of the global sliding surfaces σ_1 and σ_2 to origin $\sigma_1 = 0$, $\sigma_2 = 0$.

Proof We now consider a Lyapunov function candidate as follows:

$$V_2(\sigma) = (1/2)(\sigma_1^2 + \sigma_2^2).$$

The time derivative of $V_2(\sigma)$ is written by using Eqs. (19) and (23) as the following forms

$$\dot{V}_2(\sigma) = \sigma_1\dot{\sigma}_1 + \sigma_2\dot{\sigma}_2 = \sigma_1\left(G_1\left(\dot{s}_1 + a_1 s_1(0)\,\mathrm{e}^{-a_1 t}\right)\right) + \sigma_2\left(G_2\left(\dot{s}_2 + a_2 s_2(0)\,\mathrm{e}^{-a_2 t}\right)\right)$$
$$= \sigma_1\left(G_1\left(\dot{e}_1 + k_1 e_1 + b y_3 e_2 - d e_4 + a_1 s_1(0)\,\mathrm{e}^{-a_1 t}\right)\right) + \sigma_2\left(G_2\left(\dot{e}_3 + k_2 e_3 - b x_1 e_2 + a_2 s_2(0)\,\mathrm{e}^{-a_2 t}\right)\right), \quad (24)$$

$$\dot{V}_2(\sigma) = \sigma_1\left(G_1\left(a e_2 - y_2 y_3 - y_1 y_3 + x_2 x_3 + x_1 x_3 + d_3 - d_1 + u_1 + k_1 e_1 + b y_3 e_2 - d e_4 + a_1 s_1(0)\,\mathrm{e}^{-a_1 t}\right)\right)$$
$$+ \sigma_2\left(G_2\left(y_2^2 - c y_3^2 + y_4^2 - x_2^2 + c x_3^2 - x_4^2 + d_4 - d_2 + u_2 + k_2 e_3 + b x_1 e_2 + a_2 s_2(0)\,\mathrm{e}^{-a_2 t}\right)\right). \quad (25)$$

Using control input (23), equation (25 can be written as

$$\dot{V}_2(\sigma) = \sigma_1\left(G_1\left(d_3 - d_1 - M_1\,\mathrm{sgn}(\sigma_1)\,|\sigma_1|^{\eta_1} - \gamma_1\sigma_1 - \rho_1\tanh(\sigma_1)\right)\right)$$
$$+ \sigma_2\left(G_2\left(d_4 - d_2 - M_2\,\mathrm{sgn}(\sigma_2)\,|\sigma_2|^{\eta_2} - \gamma_2\sigma_2 - \rho_2\tanh(\sigma_2)\right)\right). \quad (26)$$

Let the disturbances be bounded as $d_1 < |L_1|$, $d_2 < |L_2|$, $d_3 < |L_3|$, $d_4 < |L_4|$, and suppose $\rho_1 \geq \max(\Lambda_1)$, $\rho_2 \geq \max(\Lambda_2)$, where

$$\begin{cases} \Lambda_1 = d_3 - d_1 = |L_3| - |L_1|, \\ \Lambda_2 = d_4 - d_2 = |L_4| - |L_2|. \end{cases} \quad (27)$$

Then, using Eq. (27), equation (26) can be written as

$$\dot{V}_2(\sigma) \leq G_1\left(-M_1|\sigma_1|^{\eta_1+1} - \gamma_1\sigma_1^2\right) + G_2(-M_2|\sigma_2|^{\eta_2+1} - \gamma_2\sigma_2^2), \quad (28)$$

$$\dot{V}_2(\sigma) \leq -\chi_1 V_2^{\overline{\eta}_1}(\sigma_1) - \psi_1 V_2(\sigma_1) - \chi_2 V_2^{\overline{\eta}_2}(\sigma_2)\psi_2 V_2(\sigma_2), \quad (29)$$

where $\overline{\eta}_1 = (\eta_1+1)/2 < 1$, $\overline{\eta}_2 = (\eta_2+1)/2 < 1$, $\chi_1 = 2^{\overline{\eta}} M_1 G_1 > 0$, $\chi_2 = 2^{\overline{\eta}} M_2 G_2 > 0$, $\psi_1 = 2\gamma_1 G_1$, $\psi_2 = 2\gamma_2 G_2$.

It is seen that the derivative of Lyapunov function V_2 is asymptotically stable. Thus, global sliding surfaces (22) are asymptotically stable and ensure that the global sliding surfaces σ_1 and σ_2 converge to $\sigma_1 = 0$ and $\sigma_2 = 0$, respectively. Hence trajectories of the slave system (17) follow the master system (16).

Usually it is assumed that the upper bound of disturbances is unknown and hence finding the actual values of the parameters ρ_1 and ρ_2 is difficult. Therefore, the adaptive tuning method is designed to determine the upper bound of the disturbances. Hence the control inputs in Eq. (23) are modified as:

$$u_1 = -k_1 e_1 - b e_2 y_3 + d e_4 - a e_2 + y_2 e_3 + x_3 e_2 + y_1 e_3 + x_3 e_1 - a_1 s_1(0)\,\mathrm{e}^{-a_1 t} - M_1\,\mathrm{sgn}(\sigma_1)\,|\sigma_1|^{\eta_1} - \gamma_1\sigma_1 - \widehat{\rho}_1\tanh(\sigma_1),$$
$$u_2 = -k_3 e_3 - b x_1 e_2 - y_2^2 + c y_3^2 - y_4^2 + x_2^2 - c x_3^2 + x_4^2 - a_2 s_2(0)\,\mathrm{e}^{-a_2 t} - M_2\,\mathrm{sgn}(\sigma_2)\,|\sigma_2|^{\eta_2} - \gamma_2\sigma_2 - \widehat{\rho}_2\tanh(\sigma_2), \quad (30)$$

where $\widehat{\rho}_1$ and $\widehat{\rho}_2$ are the estimated values of ρ_1 and ρ_2, respectively. The estimates $\widehat{\rho}_1$ and $\widehat{\rho}_2$ are done using the following adaptation rule:

$$\dot{\widehat{\rho}}_i = k_{\rho i}|\sigma_i|, \quad i = 1, 2, \quad (31)$$

where $k_{\rho i}$ is a positive constant.

Now, the stability of the sliding surfaces and their convergence to origin is ensured with the help of the following theorem.

Theorem 2 Suppose that the slave system in Eq. (17) is controlled by Eq. (30) together with the global sliding surfaces (22). Then the trajectories of the slave system (17) follow master system (16) and ensure the asymptotic convergence of the global sliding surfaces σ_1 and σ_2 to origin $\sigma_1 = 0$, $\sigma_2 = 0$.

Proof Let a Lyapunov candidate as $V_3(\sigma, \rho_i) = (1/2)\left(\sigma_1^2 + \sigma_2^2 + R_1\tilde{\rho}_1^2 + R_2\tilde{\rho}_2^2\right)$, where $\tilde{\rho}_i = \hat{\rho}_i - \rho_i$ and $R_i = 1/k_{\rho i}$, with $i = 1, 2$. The time derivative of $V_3(\sigma, \rho_i)$ using Eqs. (22) and (31) can be written as

$$\dot{V}_3(\sigma, \rho_i) = \sigma_1\left(G_1\left(\dot{s}_1 + a_1 s_1(0)\,\mathrm{e}^{-a_1 t}\right)\right) + \sigma_2\left(G_2\left(\dot{s}_2 + a_2 s_2(0)\,\mathrm{e}^{-a_2 t}\right)\right) + R_1(\hat{\rho}_1 - \rho_1)k_{\rho 1}|\sigma_1| + R_2(\hat{\rho}_2 - \rho_2)k_{\rho 2}|\sigma_2|. \quad (32)$$

Using the derivative of integral sliding surfaces (19), equation (32) can be written as

$$\dot{V}_3(\sigma, \rho_i) = \sigma_1\left(G_1\left(\dot{e}_1 + k_1 e_1 + b y_3 e_2 - d e_4 + a_1 s_1(0)\,\mathrm{e}^{-a_1 t}\right)\right) + \sigma_2\left(G_2\left(\dot{e}_3 + k_2 e_3 + b x_1 e_2 + a_2 s_2(0)\,\mathrm{e}^{-a_2 t}\right)\right) + R_1(\widehat{\rho}_1 - \rho_1)k_{\rho 1}|\sigma_1| + R_2(\widehat{\rho}_2 - \rho_2)k_{\rho 2}|\sigma_2|. \quad (33)$$

Now, using error dynamics (18) and control input (30), equation (33) can be written as

$$\dot{V}_3(\sigma, \rho_i) = \sigma_1\left(G_1\left(d_3 - d_1 - M_1\,\mathrm{sgn}(\sigma_1)|\sigma_1|^{\eta_1} - \gamma_1\sigma_1 - \rho_1\tanh(\sigma_1)\right)\right) + \sigma_2\left(G_2\left(d_4 - d_2 - M_2\,\mathrm{sgn}(\sigma_2)|\sigma_2|^{\eta_2} - \gamma_2\sigma_2 - \rho_2\tanh(\sigma_2)\right)\right) + R_1(\widehat{\rho}_1 - \rho_1)k_{\rho 1}|\sigma_1| + R_2(\widehat{\rho}_2 - \rho_2)k_{\rho 2}|\sigma_2|. \quad (34)$$

Using the boundness condition defined in Eq. (27), equation (34) can be written as

$$\dot{V}_3(\sigma, \rho_i) = \sigma_1\left(G_1\left(\Lambda_1 - M_1\,\mathrm{sgn}(\sigma_1)|\sigma_1|^{\eta_1} - \gamma_1\sigma_1 - \hat{\rho}_1\tanh(\sigma_1)\right)\right) + \sigma_2\left(G_2\left(\Lambda_2 - M_2\,\mathrm{sgn}(\sigma_2)|\sigma_2|^{\eta_2} - \gamma_2\sigma_2 - \widehat{\rho}_2\tanh(\sigma_2)\right)\right)$$

$$+R_1\left(\widehat{\rho}_1-\rho_1\right)k_{\rho 1}\left|\sigma_1\right|+R_2(\hat{\rho}_2-\rho_2)k_{\rho 2}\left|\sigma_2\right|. \tag{35}$$

Arranging the terms, we can write as

$$\begin{aligned}\dot{V}_3\left(\sigma,\rho_i\right)\leq & -G_1M_1|\sigma_1|^{\eta_1+1}-\gamma_1G_1\sigma_1^2+G_1\Lambda_1\left|\sigma_1\right|-G_1\left|\sigma_1\right|\hat{\rho}_1\\ & -G_2M_2|\sigma_2|^{\eta_2+1}-\gamma_2G_2\sigma_2^2+G_2\Lambda_2\left|\sigma_2\right|-G_2\left|\sigma_2\right|\hat{\rho}_2+R_1\left(\hat{\rho}_1-\rho_1\right)k_{\rho 1}\left|\sigma_1\right|\\ & +R_2\left(\hat{\rho}_2-\rho_2\right)k_{\rho 2}\left|\sigma_2\right|+G_1\left|\sigma_1\right|\rho_1-G_1\left|\sigma_1\right|\rho_1+G_2\left|\sigma_2\right|\rho_2-G_2\left|\sigma_2\right|\rho_2.\end{aligned} \tag{36}$$

Or equation (36) can be written as

$$\begin{aligned}\dot{V}_3\left(\sigma,\rho_i\right)\leq & -G_1M_1|\sigma_1|^{\eta_1+1}-\gamma_1G_1\sigma_1^2-\left(G_1-R_1k_{\rho 1}\right)\left(\hat{\rho}_1-\rho_1\right)\left|\sigma_1\right|-G_1\left|\sigma_1\right|\left(\rho_1-\Lambda_1\right)\\ & -G_2M_2|\sigma_2|^{\eta_2+1}-\gamma_2G_2\sigma_2^2-\left(G_2-R_2k_{\rho 2}\right)\left(\hat{\rho}_2-\rho_2\right)\left|\sigma_2\right|-G_2\left|\sigma_2\right|\left(\rho_2-\Lambda_2\right).\end{aligned} \tag{37}$$

Using $\widetilde{\rho}_i=\widehat{\rho}_i-\rho_i$, equation (37) can be written as

$$\begin{aligned}\dot{V}_3\left(\sigma,\rho_i\right)\leq & -G_1M_1|\sigma_1|^{\eta_1+1}-\gamma_1G_1\sigma_1^2-\left(G_1-R_1k_{\rho 1}\right)\left(\tilde{\rho}_1\right)\left|\sigma_1\right|-G_1\left|\sigma_1\right|\left(\rho_1-\Lambda_1\right)\\ & -G_2M_2|\sigma_2|^{\eta_2+1}-\gamma_2G_2\sigma_2^2-\left(G_2-R_2k_{\rho 2}\right)\left(\tilde{\rho}_2\right)\left|\sigma_2\right|-G_2\left|\sigma_2\right|\left(\rho_2-\Lambda_2\right).\end{aligned} \tag{38}$$

Since, $\rho_1>\Lambda_1$, $\rho_2>\Lambda_2$, and $G_1>R_1k_{\rho 1}$, $G_2>R_2k_{\rho 2}$, we can say that according to Lyapunov stability theory, Lyapunov function V_3 is asymptotically stable and ensure that the global sliding surfaces σ_1 and σ_2 converge to $\sigma_1=0$ and $\sigma_2=0$, respectively, in the presence of unknown bounded disturbances. The stability analysis of the Lyapunov function V_3 presented in the paper is done with a similar stability analysis to the ones available in Refs. [57] and [58].

Switching synchronization technique is achieved by using the following stages:

Stage 1 The chaotic behavior is achieved by the synchronization between the master and slave systems using the technique presented above.

Stage 2 The stable behavior is achieved by the synchronization but considering those parameters of the master system for which it behaves in a stable manner. One such set of parameters is $a=5$, $b=40$, $c=0.001$, $d=0.2$, and $p=0.1$.

Stage 3 The periodic behavior is achieved by the synchronization but, the value of parameter $c=0.3$ is considered for the master system and keeping other parameters the same as before.

Stage 4 The chaotic behavior is used for the hybrid synchronization, i.e., the compete synchronization of the first and fourth states, and anti-synchronization of the second and third states. The error dynamics and control inputs for hybrid synchronization are defined in Eqs. (39) and (40), respectively. It may be noted here that the Stages 1–4 need not be in sequential order, rather it can be in any arbitrary order.

$$\begin{aligned}\dot{e}_1 &= \dot{y}_1-\dot{x}_1\\ &= ae_2-y_2y_3-y_1y_3+x_2x_3+x_1x_3+d_3-d_1+u_1,\\ \dot{e}_2 &= \dot{y}_2+\dot{x}_2=be_1y_3+bx_1e_3,\\ \dot{e}_3 &= \dot{y}_3+\dot{x}_3\\ &= y_2^2-cy_3^2+y_4^2+x_2^2-cx_3^2+x_4^2+d_4-d_2+u_2,\\ \dot{e}_4 &= \dot{y}_4-\dot{x}_4=-de_1,\end{aligned} \tag{39}$$

$$\begin{aligned}u_1 = & -k_1e_1-be_2y_3+de_4-ae_2+y_2y_3+y_1y_3-x_2x_3\\ & -x_1x_3-a_1s_1\left(0\right)\mathrm{e}^{-a_1t}-M_1\,\mathrm{sgn}\left(\sigma_1\right)|\sigma_1|^{\eta_1}\\ & -\gamma_1\sigma_1-\hat{\rho}_1\tanh\left(\sigma_1\right),\\ u_2 = & -k_3e_3-bx_1e_2-y_2^2+cy_3^2-y_4^2-x_2^2+cx_3^2-x_4^2\\ & -a_2s_2\left(0\right)\mathrm{e}^{-a_2t}-M_2\,\mathrm{sgn}\left(\sigma_2\right)|\sigma_2|^{\eta_2}-\gamma_2\sigma_2\\ & -\hat{\rho}_2\tanh\left(\sigma_2\right),\end{aligned} \tag{40}$$

where the structure of the sliding surfaces is similar to Eqs. (19), (22) and the stability of the sliding surfaces can be ensured by similar analyses as shown in Eqs. (31)–(37).

6. Results and discussion for the switching synchronization between the master system in Eq. (16) and the slave system in Eq. (17)

The initial conditions considered here for the master, slave systems, and adaptation laws are $x(0)=(0.001,\ 0.0001,\ 0.7,\ 0.01)^{\mathrm{T}}$, $y(0)=(0.1,\ 0.1,\ 1,\ -0.1)^{\mathrm{T}}$, and $\widehat{\rho}_i(0)=(0,\ 0)^{\mathrm{T}}$, respectively.

The external bounded disturbances are considered as $d_1=0.1\sin(x1)\sin(x4)+0.1\sin(t)$, $d_2=0.1\sin(x2)\sin(x3)+0.1\sin(t)$, $d_3=0.1\sin(y1)\sin(y4)+0.1\sin(t)$, $d_4=0.1\sin(y2)\sin(y4)+0.1\sin(t)$.

The parameter considered for adaptive global integral SMC for the synchronization are given here as $k_1=k_2=30$, $G_1=G_2=30$, $\beta_1=\beta_2=10$, $\gamma_1=1$, $\gamma_2=4$, $M_1=M_2=5$, $\eta_1=\eta_2=3/5$, $k_{p1}=k_{p2}=8$. These parameters are chosen to ensure the faster synchronization but with lesser and smoother control inputs.

The switching synchronization states of the master and slave systems are shown in Figs. 11 and 12, respectively. The switching synchronization errors are given in Figs. 13 and 14, respectively.

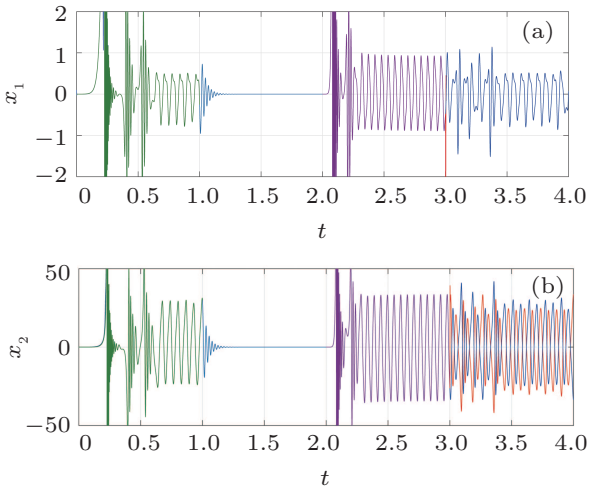


Fig. 11. (color online) Switching synchronization behaviors for the first and second states of master system (16) and slave system (17).

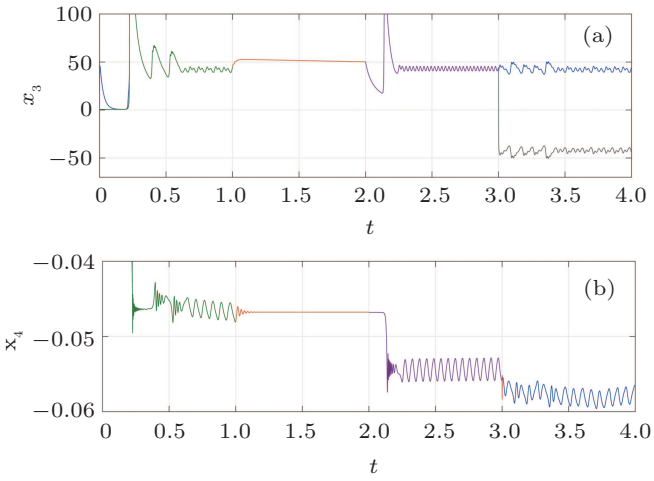


Fig. 12. (color online) Switching synchronization behaviors for the third and fourth states of master system (16) and slave system (17).

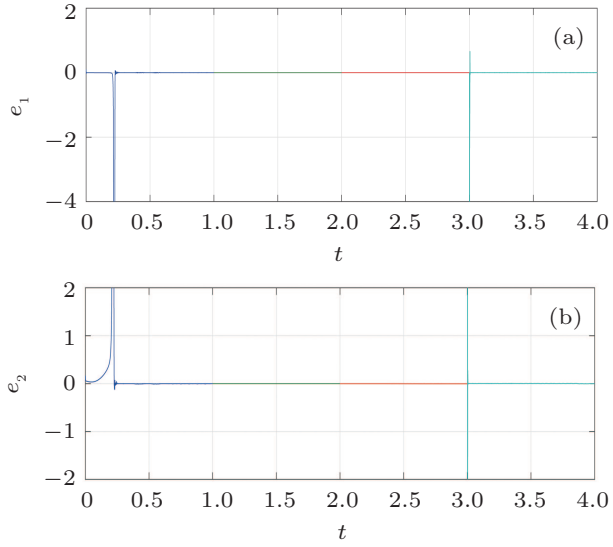


Fig. 13. (color online) Switching synchronization errors for the first and second states of master system (16) and slave system (17).

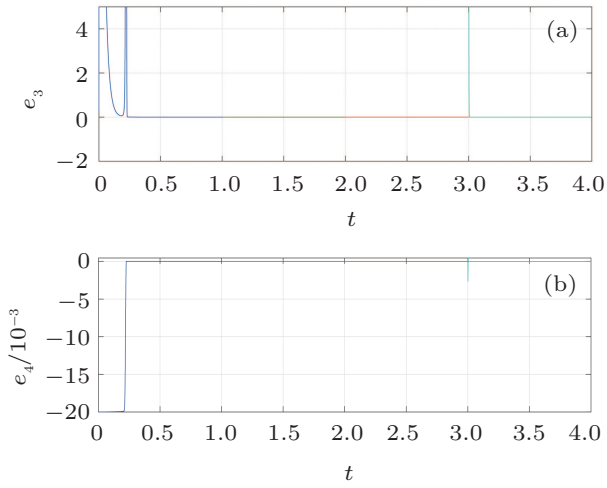


Fig. 14. (color online) Switching synchronization errors for the third and fourth states of master system (16) and slave system (17).

The behaviors of the sliding surfaces s_i and σ_i are shown in Figs. 15 and 16, respectively. The estimation of the gains of the switching control laws for the boundness of the disturbances is shown in Fig. 17.

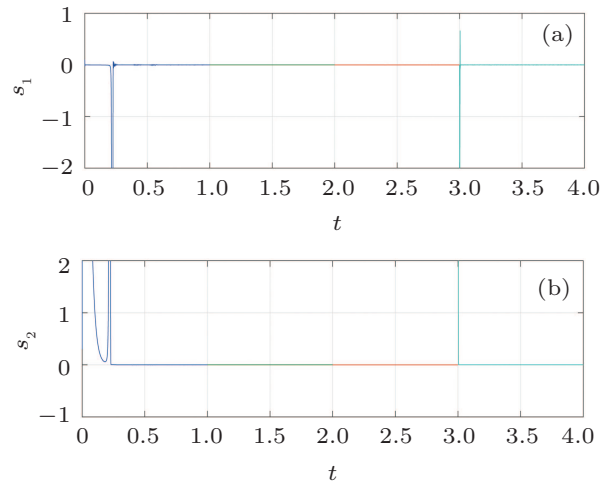


Fig. 15. (color online) Behavior of the integral sliding surfaces for the synchronization of master system (16) and slave system (17).

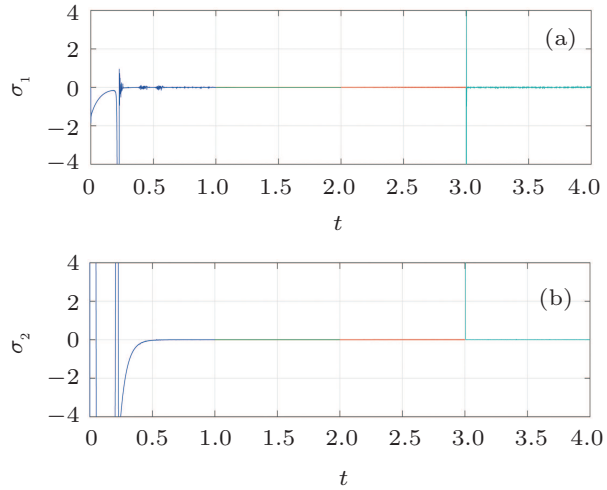


Fig. 16. (color online) Behavior of the global sliding surfaces for the synchronization of system (16) and system (17).

It is observed from Fig. 11 and Fig. 12 that during the time unit $0 < t < 1$, the synchronization is achieved for the chaotic behavior of the master system; during the time unit $1 < t < 2$, the synchronization is achieved for the stable behavior; during the time unit $2 < t < 3$, the synchronization is achieved for the periodic behavior; and during the time unit $3 < t < 4$, the hybrid synchronization is achieved. During hybrid synchronization the first and fourth states are synchronized, and the second and third states are anti-synchronized. It is noted from Fig. 13 and Fig. 14 that the synchronization errors converge to zero in a very short time interval. It is visual from Fig. 15 and Fig. 16 that the reaching time to the sliding surfaces is less and also chattering is negligible.

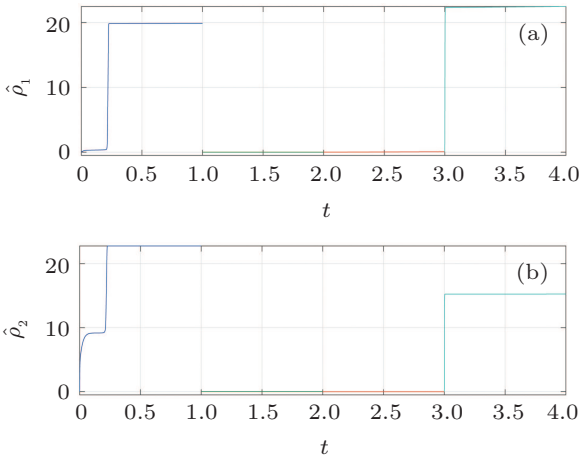


Fig. 17. (color online) Estimation of the gains of the boundness of disturbances for the synchronization of system (16) and system (17).

7. Comparison of the performances of the controller in Ref. [54] and the controller of the present work

This section presents a comparison of the performances of the controller of the present work and the controller reported in Ref. [54].

7.1. Linear synchronization between the master and slave systems as given in Ref. [54]

The structure of master system, slave system, errors, and controller designed in Ref. [54] are rewritten respectively in the following equations.

$$\begin{cases} \dot{x}_1 = a x_2 x_3, \\ \dot{x}_2 = 1 - m x_3^2, \\ \dot{x}_3 = x_1 + a x_2 x_3 + c; \end{cases} \tag{41}$$

$$\begin{cases} \dot{y}_1 = k_1 a (y_2 - b_2)(y_3 - b_3) k_2^{-1} k_3^{-1} + d_1 + u_1, \\ \dot{y}_2 = k_2 - k_2 m (y_3 - b_3)^2 k_3^{-2} + d_2 + u_2, \\ \dot{y}_3 = k_3 k_1^{-1} (y_1 - b_1) + k_1^{-1} (y_2 - b_2)(y_3 - b_3) \\ \qquad + c k_3 + d_3 + u_3; \end{cases} \tag{42}$$

$$\begin{cases} e_1 = y_1 - (k_1 x_1 + b_1), \\ e_2 = y_2 - (k_2 x_2 + b_2), \\ e_1 = y_3 - (k_3 x_3 + b_3); \end{cases} \tag{43}$$

$$\begin{cases} u_1 = -\eta e_1, \\ u_2 = -\eta e_2, \\ u_3 = -\eta e_3, \\ \dot{\eta} = e_1^2 + e_2^2 + e_3^2, \end{cases} \tag{44}$$

where the initial conditions, and parameters of systems and controllers are considered to be the same as those in Ref. [54] and are given as $x_0 = (0.1,\ 0.1,\ 0.1)^{\mathrm{T}}$, $y_0 = (-0.1,\ 0.2,\ -0.1)^{\mathrm{T}}$, $\eta_0 = 0$, $k_1 = -1$, $k_2 = 2$, $k_3 = 1$, $a = 1$, $m = 1$, $c = 1$.

7.2. Synchronization between chaotic systems of Ref. [54] by using the adaptive global integral SMC

The structure of the master system, slave system, errors, sliding surfaces, and controller designed using the adaptive global integral SMC, i.e., the controller designed in the present work, are shown below.

$$\begin{cases} \dot{x}_1 = a x_2 x_3, \\ \dot{x}_2 = 1 - m x_3^2, \\ \dot{x}_3 = x_1 + a x_2 x_3 + c; \end{cases} \tag{45}$$

$$\begin{cases} \dot{y}_1 = a y_2 y_3, \\ \dot{y}_2 = 1 - m y_3^2 + d_2 + u_1, \\ \dot{y}_3 = y_1 + a y_2 y_3 + c + d_3 + u_2; \end{cases} \tag{46}$$

$$\begin{cases} s_1 = e_2 + \displaystyle\int_0^{\tau} (k_{1s} e_2 - a x_3 e_1), \\ s_2 = e_3 + \displaystyle\int_0^{\tau} (k_{2s} e_3 + a y_2 e_1), \\ \sigma_1 = G_1 \left(s_1(t) - s_1(0)\, \mathrm{e}^{-\beta_1 t} \right), \\ \sigma_2 = G_2 \left(s_2(t) - s_2(0)\, \mathrm{e}^{-\beta_2 t} \right); \end{cases} \tag{47}$$

$$\begin{cases} u_1 = m \left(y_3^2 - x_3^2 \right) - k_{1s} e_2 + a x_3 e_1 - \beta_1 s_1(0)\, \mathrm{e}^{-\beta_1 t} \\ \qquad - \hat{\rho}_1 \tanh(\sigma_1), \\ u_2 = -e_1 - a y_2 e_3 - a x_3 e_1 - k_{2s} e_3 - \beta_2 s_2(0)\, \mathrm{e}^{-\beta_2 t} \\ \qquad - \hat{\rho}_2 \tanh(\sigma_2), \\ \dot{\hat{\rho}}_1 = k_{p1} |s_1|, \\ \dot{\hat{\rho}}_2 = k_{p2} |s_2|. \end{cases} \tag{48}$$

The initial conditions considered for simulation of the synchronization between the master system (45) and slave system (46) by using the adaptive global integral SMC (47) are the same as those in Ref. [54], i.e., $x_0 = (0.1,\ 0.1,\ 0.1)^{\mathrm{T}}$, $y_0 = (-0.1,\ 0.2,\ -0.1)^{\mathrm{T}}$, $a = 1$, $m = 1$, $c = 1$, and the parameters of the controllers are considered as $k_{1s} = 2.5$, $k_{2s} = 2$, $\beta_1 = 1.6$, $\beta_2 = 1.6$, and $G_1 = G_2 = 6$.

The performances of these two controllers are compared in the absence and presence of the matched disturbances and

are shown below. The disturbances $d1$, $d2$, $d3$ and $d2$, $d3$ added in the slaves systems (42) and (46), respectively, are given in the following equation

$$\begin{cases} d1 = 0.2\sin(x_1), \\ d2 = 0.2\sin(x_2), \\ d3 = 0.2\sin(x_3). \end{cases} \tag{49}$$

7.3. Comparison of the synchronization results when $d1 = d2 = d3 = 0$ in slave systems (42) and (46)

Here, the comparison between the performances of the controller in Ref. [54] and the controller designed in the present work is shown in the absence of disturbances. The synchronization of the states of masters (41), (45), and slaves (42), (46) is given in Fig. 18. The synchronization errors in the absence of disturbances between the states of master systems (41), (45) and slave systems (42), (46) are shown in Fig. 19. It is seen from Figs. 18(a)–18(c) that states of master system (41) and slave system (42) are not synchronized properly by using the controller[54] given in Eq. (44). But, using the controller of the present work, the states of master system (45) and slave system (46) are synchronized properly as shown in Figs. 18(d)–18(f). It is seen from Fig. 19 that the synchronization error is the same by using both the controllers.

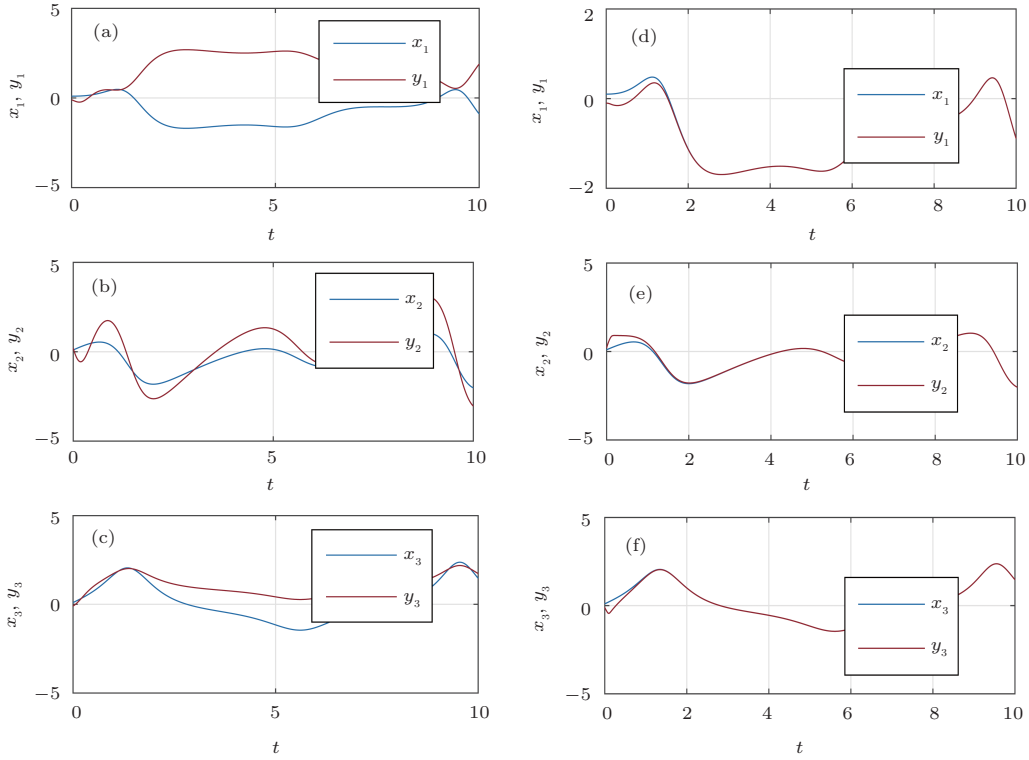


Fig. 18. (color online) Synchronization of states in absence of disturbances between the states of master systems (41), (45) and slave systems (42), (46) by using: (a)–(c) the controller of Ref. [54] and (d)–(f) the controller designed in the present work.

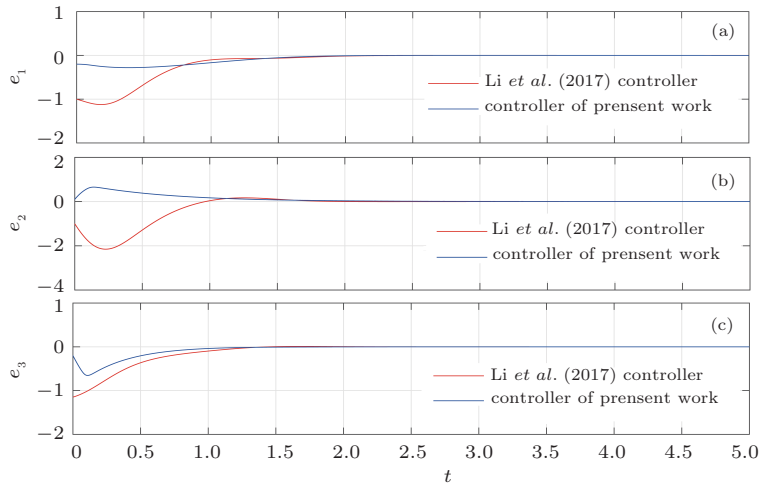


Fig. 19. (color online) Synchronization errors in the absence of disturbances between the states of master systems (41), (45) and slave systems (42), (46) by using: (a)–(c) the controller of Ref. [54] and (d)–(f) the controller designed in the present work.

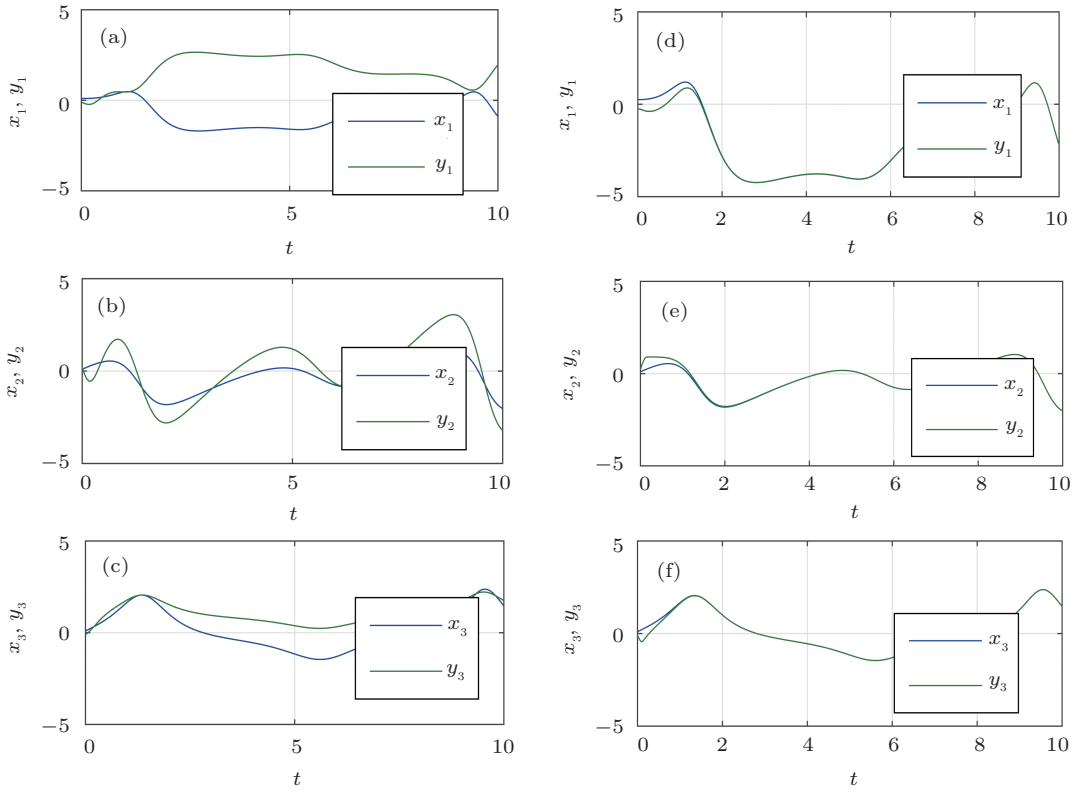


Fig. 20. (color online) Synchronization in the presence of disturbances between the states of master (41), (45) and slave (42), (46) systems by using: (a)–(c) the controller of Ref. [54] and (d)–(f) the controller designed in the present work.

7.4. Comparison of the synchronization results in the presence of disturbances for both the controllers

The robustness of synchronization in the presence of disturbances between the controller designed in Ref. [54] and the controller of the present work is compared. Synchronization of the states of master (41), (45, and slave (42), (46) systems is shown in Fig. 20. It is noted from Figs. 20(a)–20(c) that states of master (41) and slave (42) systems are not properly synchronized by using the controller[54] given in Eq. (44). But, using the controller of the present work, the states of master (45) and slave (46) systems, as shown in Figs. 20(d)–20(f), are synchronized properly. It is apparent from Fig. 21 that the steady state synchronization error is very high in the results obtained by using the controller of Ref. [54], whereas the same is absent using the controller designed in the present work. Thus, the controller designed in the present paper performs better than that designed in Ref. [54].

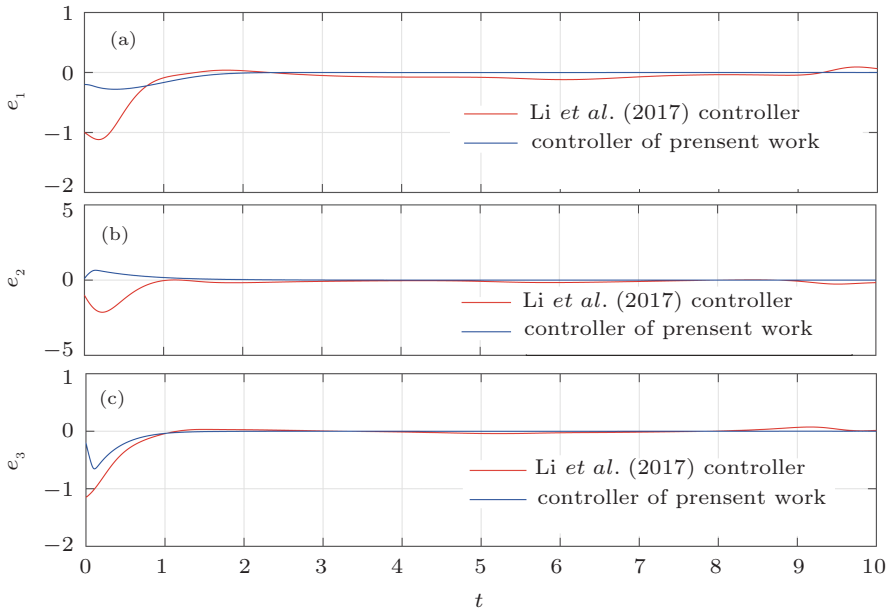


Fig. 21. (color online) Synchronization errors in the presence of disturbances between the states of master (41), (45) and slave (42), (46) systems by using: (a)–(c) the controller of Ref. [54] and (d)–(f) the controller designed in the present work.

8. Conclusions

In this paper, a new 4D chaotic system having the largest first positive Lyapunov exponent is reported. The largest first positive Lyapunov exponent of the new system is compared with many reported systems (3D and 4D chaotic systems) in the literature. The proposed system has a hyperbolic curve and circular paraboloid types of equilibria along with coexistence of chaotic attractors and hyperchaotic behavior. The simulation results confirm the claims about the system. Further, the circuit implementation results validate the chaotic nature of the system. The proposed system may be more suitable for secure communication since it has the largest first Lyapunov exponent. Switching synchronization phenomenon is proposed for the new chaotic system. An adaptive global integral sliding mode control is designed for the switching synchronization. The switching synchronization is achieved in four stages. These are (i) chaotic behavior, (ii) stable behavior, (iii), periodic behavior, and (iv) hybrid synchronization.

References

[1] Chen S H and Tong P 2017 *Chin. Phys. B* **26** 050503
[2] Wang L F, Jia Y and Qiu K 2017 *Chin. Phys. B* **26** 030503
[3] Zhang H X and Lei Y M 2017 *Chin. Phys. B* **26** 030502
[4] Gan Z H, Chai X L and Chen Y R 2017 *Chin. Phys. B* **26** 020504
[5] Gholamin P and Sheikhani A H Refahi 2017 *Chin. J. Phys.* **55** 1300
[6] Afari M A, Mliki E, Akgul A, Pham V T, Kingni S T, Wang X and Jafari S 2017 *Nonlinear Dyn.* **88** 28
[7] Wang Z, Akgul A, Pham V T and Jafari S 2017 *Nonlinear Dyn.* **89** 1
[8] Pham V T, Volos C, Jafari S and Kapitaniak T 2016 *Nonlinear Dyn.* **87** 2001
[9] Sprott J C 2003 *Chaos and time-series analysis* (Oxford: Oxford University Press)
[10] Singh J P and Roy B K 2016 *Chaos, Solitons and Fractals* **92** 73
[11] Wei Z, Moroz I, Sprott J C, Akgul A and Zhang W 2017 *Chaos* **27** 033101
[12] Qi G, Chen G and Zhang Y 2008 *Chaos, Solitons and Fractals* **37** 409
[13] Wei Z, Pham V T, Kapitaniak T and Wang Z 2016 *Nonlinear Dyn.* **85** 1635
[14] Wei Z, Moroz I, Wang Z, Sprott J C and Kapitaniak T 2016 *Int. J. Bifur. Chaos* **26** 1650125
[15] Wei Z, Yu P, Zhang W and Yao M 2015 *Nonlinear Dyn.* **82** 131
[16] Kiseleva M A, Kuznetov N V and Leonov G A 2016 *IFAC-Papers On-Line* **49** 051
[17] Wei Z, Moroz I, Sprott J C, Wang Z and Zhang W 2017 *Int. J. Bifur. Chaos* **27** 1730008
[18] Singh J P and Roy B K 2016 *Optik* **127** 11982
[19] Leonov G A, Kuznetsov N V and Vagaitsev V I 2011 *Phys. Lett. A* **375** 2230
[20] Leonov G A, Kuznetsov N V, Kuznestova O A, Seledzhi S M and Vagaitsev V I *Trans. Syst. Control* **6** 1
[21] Leonov G A, Kuznetsov N V and Vagaitsev V I 2012 *Physica D* **241** 1482
[22] Wei Z and Zhang W 2014 *Int. J. Bifur. Chaos* **24** 1450127
[23] Pham V T, Volos C S, Jafari S, Wei Z and Wang X 2014 *Int. J. Bifur. Chaos* **24** 1450073
[24] Leonov G A and Kuznetsov N V 2013 *Int. J. Bifur. Chaos* **23** 1330002
[25] Leonov G A, Kuznetsov N V, Kiseleva M A, Solovyeva E P and Zaretskiy A M 2014 *Nonlinear Dyn.* **77** 277
[26] Pham V T, Jafari S, Volos C, *et al.* 2016 *IEEE Trans. Circ. Syst. II: Express Briefs* **63** 878
[27] Kuznetsov N V, Mokaev T N and Vasilyev P A 2014 *Commun. Nonlinear Sci. Numer. Simul.* **19** 1027
[28] Jafari S, Sprott J C and Molaie M 2016 *Int. J. Bifur. Chaos* **26** 1650098
[29] Zhou P and Yang F 2014 *Nonlinear Dyn.* **76** 473
[30] Li C, Sprott J C and Thio W 2014 *J. Exp. Theor. Phys.* **118** 494
[31] Chen Y and Yang Q 2015 *Math. Comput. Simul.* **112** 40
[32] Ma J, Chen Z, Wang Z and Zhang Q 2015 *Nonlinear Dyn.* **81** 1275
[33] Li Q, Hu S, Tang S and Zeng G 2014 *Int. J. Circ. Theory Appl.* **42** 1172
[34] Shen C, Yu S, Lü J and Chen G 2014 *IEEE Trans. Circ. Syst. I: Regular Papers* **61** 854
[35] Shen C, Yu S, Lü J and Chen G 2014 *IEEE Trans. Circ. Syst. I: Regular Papers* **61** 2380
[36] Zhou L, Wang C and Zhou L 2017 *Int. J. Bifur. Chaos* **27** 1750027
[37] Ma J C, Wang Z Q and Zhang Q 2015 *Nonlinear Dyn.* **81** 1275
[38] Yalçin M E, Suykens J A K and Vewalle J 2000 *Nonlinear Dyn. Electron. Syst.* **25**
[39] Li Y, Tang W K S and Chen G 2005 *Int. J. Circ. Theory Appl.* **33** 235
[40] Li C and Sprott J C 2014 *Phys. Lett. A* **378** 178
[41] Khan S A 2010 *Indian Association of Physics Teachers* **2** 327
[42] Wolf A, Swift J B, Swinney H L and Vastano J A 1985 *Physica D* **16** 285
[43] Vaidyanathan S 2016 *Int. J. Control Theory Appl.* **9** 279
[44] Wang Z, Yuan J and Wei J 2017 *Optik* **137** 85
[45] Mobayen S and Baleanu D 2016 *Nonlinear Dyn.* **83** 1557
[46] Singh P P, Singh J P and Roy B K 2014 *Chaos, Solitons and Fractals* **69** 31
[47] Singh P P, Singh J P and Roy B K 2017 *IETE J. Res.* **17**
[48] Pecora L M and Carroll T L 2015 *Chaos* **25** 097611
[49] Miao Q, Tang Y, Lu S and Fang J 2009 *Nonlinear Dyn.* **57** 107
[50] Kahn M A and Poria S 2013 *Pramana* **81** 395
[51] Singh J P and Roy B K 2017 *Trans. Institute of Measurement Control* **14**
[52] Chen M, Wu Q and Jiang C 2012 *Nonlinear Dyn.* **70** 2421
[53] Hu C and Yu J 2016 *Chaos, Solitons and Fractals* **91** 262
[54] Li C B, Thio W J C, Sprott J C, Zhang R X and Lu T A 2017 *Chin. Phys B* **26** 120501
[55] Zha J, Li C, Song B and Hu W 2016 *Int. J. Syst. Sci.* **47** 3952
[56] Bartolini G, Fridman L, Pisano A and Usai E 2008 *Modern Sliding Mode Control Theory* (Heidelberg: Springer-Verlag)
[57] Mobayen S and Tchier F 2017 *Int. J. Control Autom. Syst.* **15** 1097
[58] Mobayen S and Tchier F 2017 *Trans. Institute of Measurement Control*